Copper Nanoparticles with Tunable Size: Implications for Plasmonic Catalysis

Liyan Ouyang, Vincent Noël, Alexa Courty, Jean-Marc Campagne, Armelle Ouali, Emmanuel Vrancken

▶ **To cite this version:**

Liyan Ouyang, Vincent Noël, Alexa Courty, Jean-Marc Campagne, Armelle Ouali, et al.. Copper Nanoparticles with Tunable Size: Implications for Plasmonic Catalysis. ACS Applied Nano Materials, 2022, 5 (2), pp.2839-2847. 10.1021/acsanm.2c00016 . hal-03738181

HAL Id: hal-03738181
https://hal.science/hal-03738181

Submitted on 25 Jul 2022

HAL is a multi-disciplinary open access archive for the deposit and dissemination of scientific research documents, whether they are published or not. The documents may come from teaching and research institutions in France or abroad, or from public or private research centers.

L'archive ouverte pluridisciplinaire **HAL**, est destinée au dépôt et à la diffusion de documents scientifiques de niveau recherche, publiés ou non, émanant des établissements d'enseignement et de recherche français ou étrangers, des laboratoires publics ou privés.

Copper Nanoparticles with Tunable Size: Implications for Plasmonic Catalysis

Liyan Ouyang,[1] Vincent Noël,[2] Alexa Courty,[,3] Jean-Marc Campagne,[1] Armelle Ouali,[*,1] Emmanuel Vrancken[*,1]*

[1] Institut Charles Gerhardt Montpellier, Univ. Montpellier, CNRS, ENSCM, Montpellier, France

[2] Université de Paris, ITODYS, CNRS, F-75006 Paris, France

[3] Sorbonne Université, MONARIS, UMR8233, UMR 8233, F-75005 Paris, France

KEYWORDS: copper nanoparticle, scalable synthesis, thermal decomposition, organocopper reagents.

ABSTRACT: A new access to copper(0) nanoparticles (CuNPs) from readily available organocopper reagents is reported. This original amine-free methodology proves to be practical, fast and highly reproducible. It yields spherical CuNPs with an excellent control of their size and shape. These CuNPs are fully characterized by electronic microscopy (TEM, HRTEM), X-Ray photoelectron spectroscopy (XPS), X-ray diffraction (XRD), and UV-Vis spectroscopy. The size of the synthesized nanoparticles is in a size range of 5–9 nm. The reactional pathway is studied and shows a two-step process implying the formation of a primitive bulk composed of spheroid CuNPs followed by a reorganization step induced by a thiol additive and leading to the final NPs.

The robustness of this convenient protocol enables decigram scale synthesis of CuNPs without altering their size and morphology, which makes it a preparative method of choice for their synthesis. This protocol allows the rational design of future copper-based catalysts. The importance of controlling several physicochemical parameters such as size, composition, and shape in metal nanomaterials is indeed widely reported. The results presented here offer many prospects for the rapidly developing field of copper plasmonic catalysis.

1. Introduction

Metal nanoparticles (NPs) attracted growing interest due to their outstanding applications in numerous fields including catalysis,[1,2] energy conversion,[3] photonics,[4] imaging,[5] sensing,[6,7] biomedical activies[8] or nanomedicine,[9-11] to name a few. Their properties are determined by their size, their shape and their composition.[12,13] Copper is a cheap and earth-abundant metal which enables its extensive use for numerous applications, particularly in nanotechnology.[14-16] Copper nanoparticles (CuNPs) are of special interest in various fields such as biosensing[17-18] and plasmonics.[19-20] Copper is indeed a "plasmonic" metal like silver and gold, its surface plasmon resonance is also intense and narrow but slightly different (red shifted) which gives it an original sensitivity and selectivity.[21] CuNPs also generate an exciting research activity up to tremendous expectations it evokes in the field of catalysis.[15,22,23] Combined with its ability to capture light and its catalytic performance, Cu NPs provide a promising platform for efficient light-driven chemical reaction. Plamonic catalysis of non-noble metals has indeed emmerged as a unique strategy for controlling conversion percentage, improving selectivity and driving reaction under mild conditions.[24-26]

Among the different methods reported in the literature,[15] two common chemical methods involving copper(I) precursors include the disproportionation route[27-31] and the reductive pathway

from copper(I) or copper(II) salts using dihydrogen gas[32] or organic reductants, as for example borane derivatives,[33,34] amines[35] or hydrazine.[36] The disproportionation reaction enables the formation of CuNPs of various controlled morphologies but the theoretical yield is inherently limited to 50% and an excess of alkylamines of high molecular weight is required.[27-31] The reductive methods (boranes, H_2) are not restricted in terms of yield but, so far, no large-scale synthesis of CuNPs has been reported using these methodologies.[32-36] However, to be able to develop their applications, particularly the industrial ones, CuNPs must be able to be produced in large quantities with tunable sizes and with low environmental and economic cost. It is thus desirable to design simple, practical and cost-effective access to CuNPs with well-defined size and shape in a greener way.

In this work, we report an innovative, convenient and scalable method for the synthesis of spherical CuNPs with tunable size (from 5.4 to 8.5 nm) with a low size dispersity starting from simple and readily available organocopper reagents.

2 Experimental

2.1 Materials

Commercial reagents were used without further purification, except stated otherwise, and stored in a glovebox in order to avoid any traces of moisture or air contamination. The following chemicals were purchased from SIGMA: copper(I) chloride (CuCl 99.99 %), Butylmagnesium chloride solution (*n*-BuMgCl, 2.0 M solution in THF), triphenylphosphine (99 %), 1-dodecanethiol (≥ 98 %). THF was distilled over sodium/benzophenone and handled under an

atmosphere of nitrogen. The CuNPs synthesis was carried out under nitrogen atmosphere using a Schlenk line.

2.2 Characterization methods

The morphology of CuNPs was analyzed by TEM using a JOEL 1200 EX microscope with an accelerating voltage of 120kV. All CuNPs samples were prepared by dropping the nanoparticles suspensions in hexane or chloroform onto a conventional carbon-coated nickel grid, then dried on the surface of the grid under inert gas. For each sample, TEM images were taken from different parts of the grid and used to estimate size distribution of copper nanoparticles. High-resolution TEM (HRTEM) images and selected area electron diffraction (SAED) patterns were collected on a JOEL 2200FS TEM at 200KV. Image J software was used for measuring the size of nanoparticles around 300-500 NPs and the size distribution was determined using the Origin-Pro 9.1. The UV-Vis spectroscopy was performed on a V-770 UV-Visible/NIR spectrophotometer at room temperature with the wavelength range of 300 to 800 nm. Before each run, background subtraction was performed with the solvent system of choice. The measurements were performed in a quartz cell with 1cm optical path length. The experimental XPS spectra were recorded using a K-Alpha$^+$ system (Thermo Fisher Scientific, East-Grinsted, UK) fitted with a micro-focused and monochromatic Al K_α X-ray source (1486.6 eV, spot size of 400 μm). The spectrometer pass energy was set to 150 and 40 eV for the survey and the narrow high-resolution regions, respectively. Spectral calibration was determined by setting the main C_{1s} component at 285 eV. The samples were prepared by depositing several drops of the solution on a silicon wafer. TEM images were recorded prior to XPS analysis to ensure that individual nanoclusters are actually present. In this study, the surface characterization of elements of Cu, P, S, Mg, C, and Cl of CuNPs

was performed. Powder XRD pattern were collected with Ni-filtered Cu $K_{\alpha 1/\alpha 2}$ (λ = 1.5418 Å) radiation in a reflection geometry on a Pananalytical X'Pert Pro-MPD diffractometer, operating at a working voltage and current of 45 KV and 20 mA. In preparing the sample, the powder sample was formed by precipitating of nanoparticles with ethanol and centrifuging at 4000 rpm for 10 min before drying at room temperature in an N_2-filled glovebox. The dry precipitate was pulverized and the resulting powder was used to fill a glass plate.

The typical procedure was removed from here.

3 Results and discussion

3.1 State of the art

Organocopper reagents are widely used in organic synthesis and are routinely obtained by transmetalation reactions of the corresponding organo-magnesium (Grignard reagent), organo-lithium or organo-zinc precursor by a Cu(I) salt at low temperature,[37-40] as depicted in Scheme 1, eq. 1. Those species are known to be thermally unstable and to decompose at low temperature, generally between – 90 °C and 0 °C depending on the nature of the organic moiety. In the early seventies Whitesides[41] and Kochi[42] independently investigated the decomposition reactions of these alkyl copper species, followed by others.[43-45] They showed that this thermolysis reaction yield an equimolar amount of alkane and terminal alkene, aside two equivalents of metallic copper (Scheme 1, eq. 2). However, the exact nature of this metallic copper product has not been determined and, despite the interest of these seminal results, these works were not continued.

Scheme 1. Synthesis and thermolysis studies of organocopper compounds

eq.1 $RM + CuX \xrightarrow[\text{low temperature}]{\text{THF or } Et_2O} RCu + MX$

M = Li, ZnX, MgX; X = Cl, Br, I

eq.2 $2\ CH_3CH_2CH_2Cu \xrightarrow[\text{THF, 0 °C}]{} CH_3CH{=}CH_2 + CH_3CH_2CH_3 + 2\ Cu(0)$

3.2 Synthesis of CuNPs by thermolysis reaction

In an endeavor to develop a convenient, robust and scalable synthesis of CuNPs, we decided to explore the potential of the organocopper thermolysis reactions by setting up the experimental one pot procedure described in Scheme 2:

Scheme 2. Schematic representation of our experimental one pot procedure.

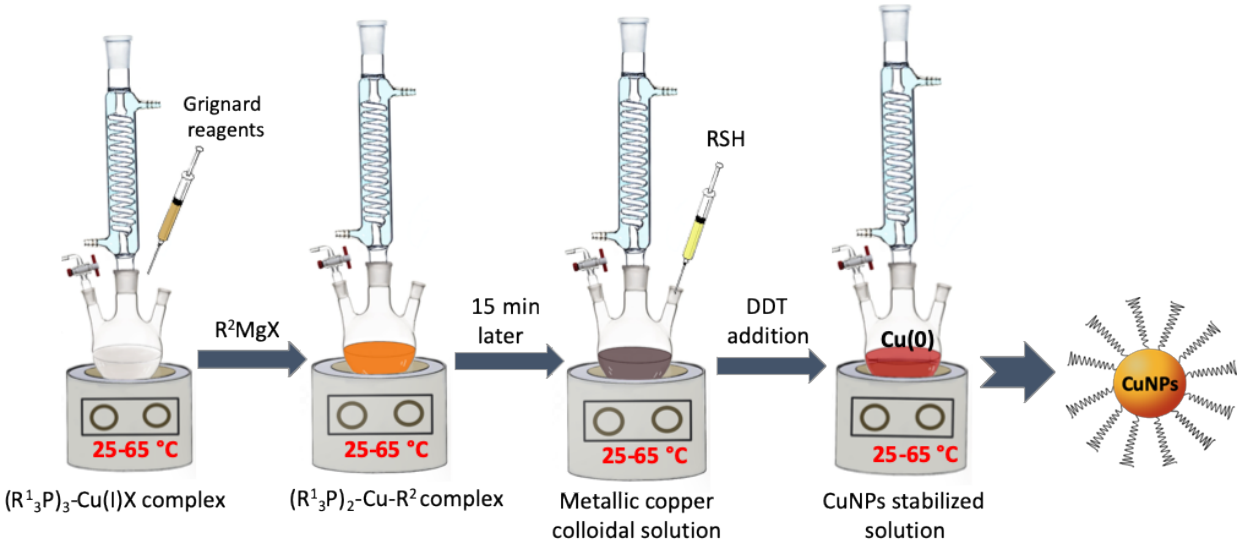

In a first try, copper chloride (1 mmol) and triphenylphosphine (3 mmol) have been stirred in dry THF (10 mL) at room temperature under inert atmosphere to generate the corresponding

copper complex $Cu(PPh_3)_3Cl$. Next *n*-BuMgCl (1 mmol) was introduced and the solution instantly turned black. After 15 minutes, dodecanethiol (DDT, 4 mmol) was added in order to prevent the precipitation of copper metal. This addition induced an immediate color change from black to red. The solution was stirred one more hour at room temperature. After standard work-up of washing / centrifugation sequences, a deep purple powder was obtained whose TEM images revealed spherical NPs with an average size of 5.4 nm ± 0.5 nm (Figure 1a and SI, Figure S1a). The same reaction was performed in refluxing THF as the reaction temperature is one of the major parameters enabling the size control of nanoparticles.[46] Under these conditions, the formation of quite monodisperse NPs with a slight increase in the size (with an average diameter of 5.6 nm ± 0.6 nm) was observed (Figure 1b and Figure S1b). An increase of the temperature from rt to 65 °C had thus not significant influence on the size of NPs. In both cases, some coalescence could be observed on the TEM images possibly indicating a ligand default. The influence of the amount of phosphine ligand was thus addressed and the 1 mmol scale synthesis were achieved at rt or in refluxing THF, and in the presence of 1 or 5 phosphine equivalents as compared to copper. The use of one equivalent of phosphine lead to polydisperse NPs whatever the temperature (Figure S2). When performing the synthesis at room temperature with 5 equivalents of phosphine, the formation of a gel was observed that prevents the isolation of NPs. Conversely, well-defined NPs were obtained in refluxing THF with a mean size of 8.5 nm ± 0.4 nm, which corresponds to a significant increase of the size with an improved size dispersity as compared to the use of 3 equivalents (5% polydispersity as compared to 9-10%, Figure 1c). The optimized temperature and Cu-to-phosphine ratio were thus 65 °C and 1 to 5 respectively (Scheme 3). The maximum of the SPR band was found at 585 nm (Figure 1d), in agreement with pure copper NPs.[33,34] It is

noteworthy that this reaction has been made many times and gave highly reproducible results, which shows its robustness.

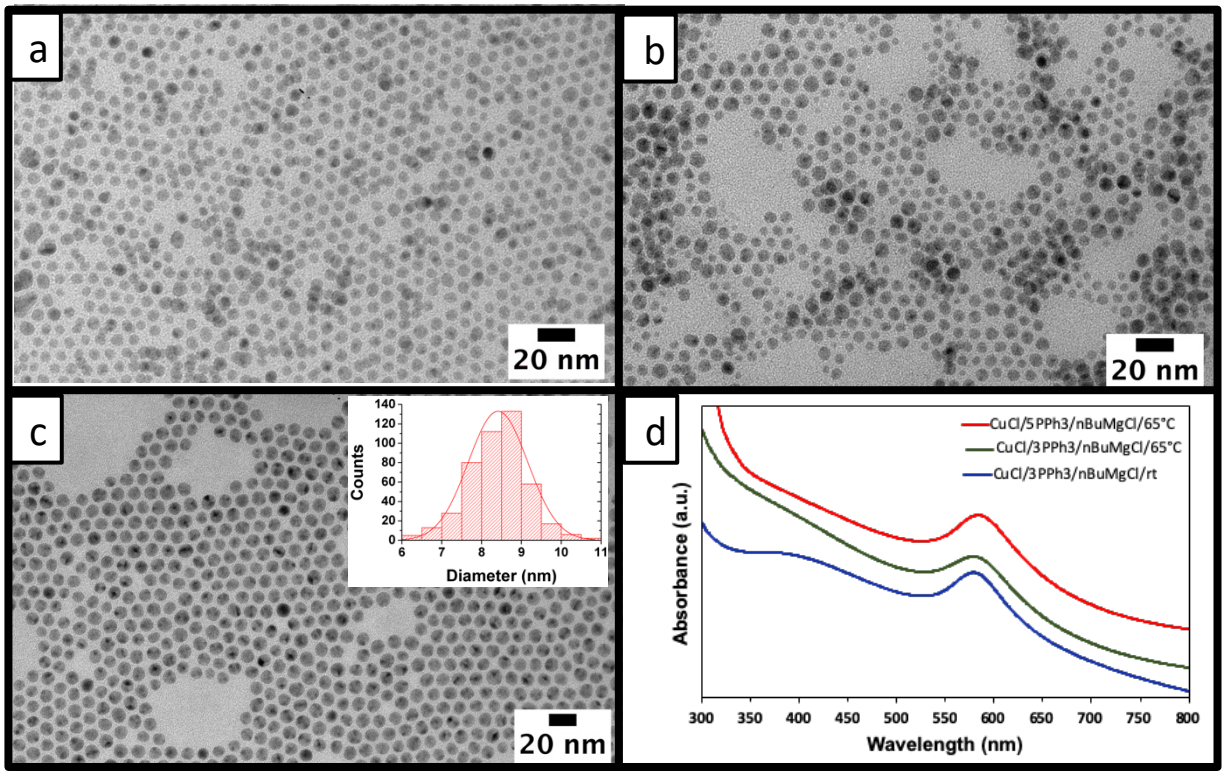

Figure 1. (a) – (c): size histograms (in inset) and TEM images of CuNPs obtained from CuCl, PPh_3 and *n*-BuMgCl in THF with: (a) Cu/PPh_3 = 1:3 at 25 °C. (b) Cu/PPh_3 = 1:3 at 65 °C. (c) Cu/PPh_3 = 1:5 at 65 °C. (d) the corresponding UV-vis absorption spectra recorded at 20 °C.

We next investigated the effect of the time between the addition of the Grignard reagent and the introduction of the DDT for a total reaction time of 1h15 (Table 1 and TEM images in Figure S3). Therefore, DDT was added after 0.5 (entry 1), 5 (entry 2) or 30 minutes (entry 4) instead of the 15 minutes used in the optimized conditions (Scheme 3).

Scheme 3. Optimized conditions for the CuNPs synthesis

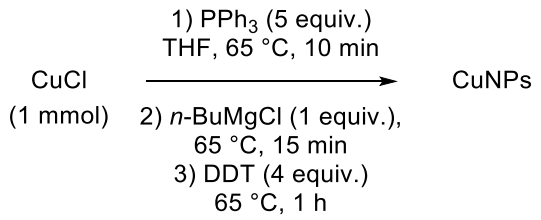

As shown in Table 1 and Figures S3a-d, achieving the addition of DDT after 0.5 or 5 minutes resulted in a slight but significant decrease of the NPs size (from 8.5 nm after 15 min. to 7.7 nm after 5 min. to 6.7 nm after 0.5 min.). On the contrary, delaying the addition to 30 minutes does not affect the morphology or the size of NPs (entry 4). Interestingly, for an addition of DDT 15 minutes after the Grignard reagent, an increase of the total reaction time to 3h15 also had no effect on the final size and shape of the NPs. (Table 1, entry 3, note [b]). Noteworthy, the addition of oleylamine or oleic acid instead of DDT in our standard reaction conditions did not lead to the formation of CuNPs.

Table 1. Influence of the time between the addition of the Grignard reagent and the introduction of the DDT (total reaction time 1h15)

Entry	Time before addition of the DDT (minutes) [a]	Cu NP size in nm	Size polydispersity in %
1	0.5	6.7 ± 0.8	12
2	5	7.7 ± 0.5	7
3	15 (reference)	8.5 ± 0.4 [b]	5[b]
4	30	8.3 ± 0.5	6

[a] The Grignard reagent is added at t = 0 [b] For a total reaction time of 3h15 instead of 1h15: 8.1 ± 0.7 nm (9%)

3.3 NP Crystallinity characterization

The NPs prepared in the optimized conditions (Figure 1c) were thus characterized by High Resolution TEM (HRTEM) imaging performed on several tens of CuNPs. The HRTEM images reveal that the NPs are well crystallized and correspond to a mixture of face centered cubic (*fcc*) single crystals (Figure 2a) and multiply twinned particles (MTP, Figure 2b). The spacing between the lattice planes (0.201 nm) deduced from the selected area electron diffraction (SAED) pattern correspond to the (111) planes of the *fcc* Cu structure (see Figure 2c and Figure S4). This synthesis method thus allows to obtain non-oxidized Cu(0) NPs. Powder X-ray diffraction analysis was next implemented in order to confirm the metallic nature of the CuNPs. Indeed, the XRD pattern (Figure 2d) shows that all the detected diffractions can be indexed to the crystal structure of zero valence copper Cu(0). The diffraction peaks located at 43.3°, 50.4°, 74.1°, 89.9° and 95.1° can be indexed to the (111), (200), (220), (311) and (222) crystal planes of *fcc* Cu (with conference to JCPDS #03-1018), respectively. No diffraction peaks characteristic of Cu_2O and/or CuO were observed, which confirms the formation of Cu(0)NPs.

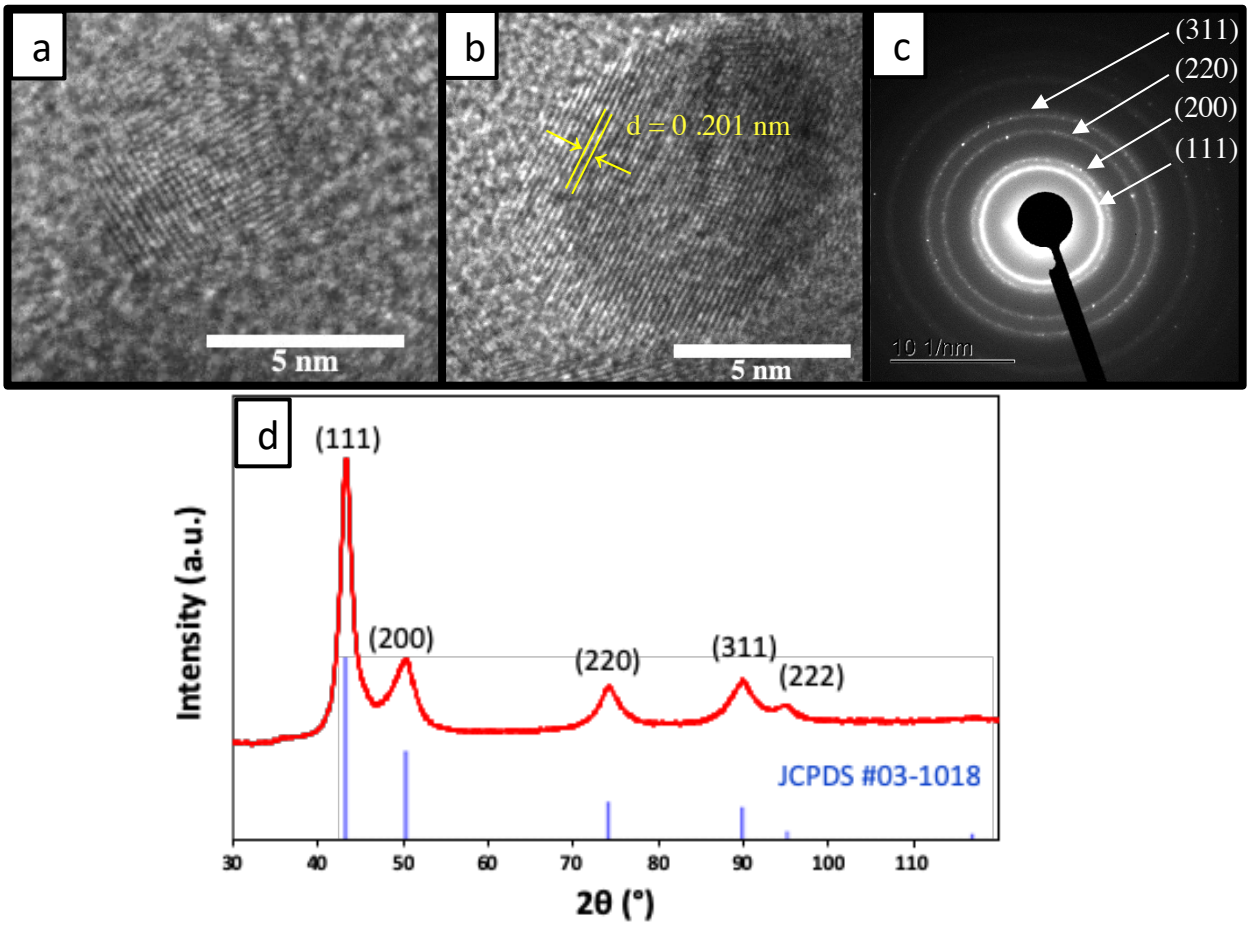

Figure 2. HRTEM images of (a) MTP's particle (b) a *fcc* single crystal (c) the corresponding SAED pattern and (d) powder XRD pattern (red: experimental, blue: theoretical) of CuNPs prepared in the optimized condition from $CuCl/PPh_3$ (5 equiv.)/*n*-BuMgCl in refluxing THF and stabilized by DDT (4 equiv.).

3.4 NP Surface characterization

Once the nature of the CuNPs cores established, XPS analysis were undertaken in order to identified the ligands present on their surface. The survey spectrum shows peaks attributed to C_{1s},

$Cu_{2p,}$ $O_{1s,}$ $S_{2p,}$ P_{2p} and small signals corresponding to Cl_{2p}, and Si_{2p} (see Table 2 and Figure S5). Theoretically, S_{2p} XPS peak is composed of two contributions, namely $S_{2p1/2}/S_{2p3/2}$, each of them characterised by a full width at half maximum (FWMH) less than 2 eV. $S_{2p1/2}/S_{2p3/2}$ contributions have commonly a relative peak intensity of ½ and a binding energy (BE) difference of 1.1 eV. Here, the S_{2p} XPS signal contains more than one $S_{2p1/2}/S_{2p3/2}$ system according to the peak shape (see Figure S5a). The main doublet at 162.5/163.4 eV, i.e. $(S_{2p1/2}/S_{2p3/2})_A$, corresponds to the Cu-S[47] bond whereas $(S_{2p1/2}/S_{2p3/2})_B$ at 163.9/165.1 eV can be attributed to unbonded thiols.[48] Fitting the S_{2p} peak using four components is not accurate enough to obtain a quantitative interpretation of the spectra. However, the relative contribution of the two systems to the sulfur XPS signal can be estimated from peak areas and leads to a ratio of Cu-S/free SH between 2 and 3 depending on the fixed fitting parameters. Consequently, the relative content of sulfur in the overall sample, i.e. the atomic percentage (At%) of thiol bonded to CuNPs, is estimated to be between 2% and 3%. P_{2p} trace (%AtP < 0.1) can be also observed at 131 eV[49] a position that matches the theoretical one for a phosphine function. According to the ratio between atomic percentage of P and S_{162eV}, the content of DDT is at least 1 order of magnitude higher than that of triphenylphosphine in the NP vicinity. Figure 2c presents the XPS spectra in the 930-970 eV range. The two main observed contributions correspond to the $Cu_{2p1/2}$ (532 eV) and the $Cu_{2p3/2}$ (950 eV) BE[50]. The presence of Cu(0) and Cu(II) on the surface has been deduced from a deconvolution of the Cu_{2p} signal using two different contributions: the first one at 932.4 eV (Cu(0) or Cu(I)) and the second one at 934.1 eV (for Cu(II)). The signal of Cu(II) was attributed to CuO (see Fig. S7 and Table S1). This may be explained by an air-driven oxidation process that occurred during the time of the XPS analysis.

Table 2. XPS data analysis

Element		Peak BE (eV)	FWHM (eV)	Area (CPS.eV)	Atomic %
C_{1s}		285.00	1.56	127089	67
Cl_{2p}		199.59	0.29	2835	0.5
Cu_{2p}		932.80	3.39	591049	21
O_{1s}		530.69	3.37	31870	7
P_{2p}		131.00	0.42	821	<0.1
S_{2p}		163.00	3.27	16703	4.34
A	*(S2p$_{1/2}$)*	*162.27*	*1.63*	*3712.22*	-
	(S2p$_{3/2}$)	*163.44*	*1.64*	*1854.60*	-
B	*(S2p$_{1/2}$)*	*163.97*	*1.86*	*1993.72*	-
	(S2p$_{3/2}$)	*165.14*	*1.86*	*997.21*	-

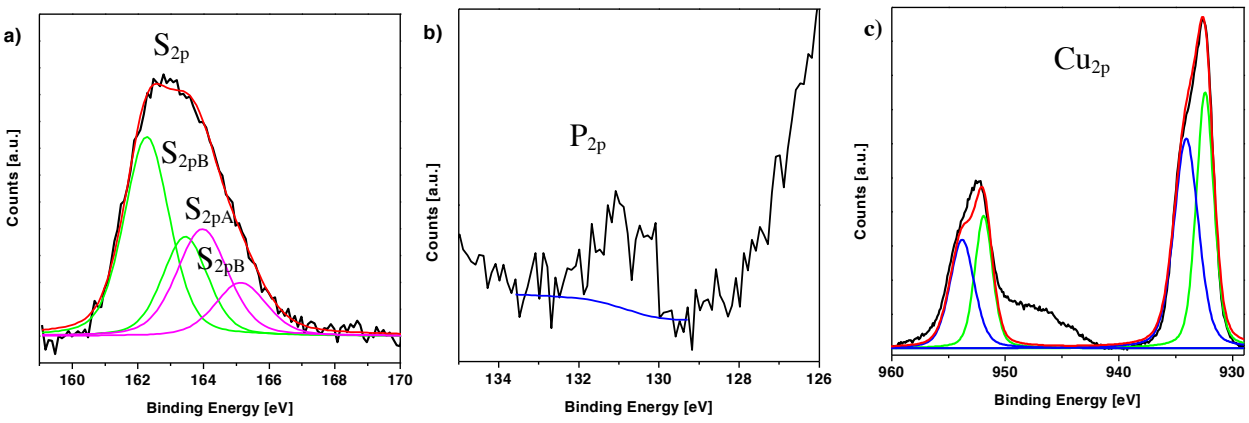

Figure 3: XPS. High resolution XPS spectra of (a) S_{2p} showing (red curve) simulated spectra from the fitting with (green and magenta curves) two doublets (b) P_{2p}; due to the low P content, P_{2p} is presented before (blue curve) baseline correction; (c) Cu_{2p}.

3.5 Decigram scale synthesis

When we undertook this study, our original requirements were to develop a reliable and practical procedure for the preparation of CuNPs of well-defined shape and size. Having achieved these objectives, it remained at this stage to check that it could be implemented on decigram scale without loss of yield and / or morphological control. The reaction has thus been performed at 5 mmol scale in the optimized conditions (Scheme 3), starting from 5 mmol (495 mg) of CuCl and 5 equivalents of PPh_3 in 50 mL of dry THF at 65 °C. After the successive addition of the Grignard reagent and the DDT, the red dark solution mixture was stirred at 65 °C for 1 h. A standard work up of washing / centrifugation sequences yielded a first batch of 270 mg of selected CuNPs with an average size of 8.4 ± 0.6 nm (7 % polydispersity, Figure 4a,c), very close to the results obtained at the centigram scale as c.a. 50 mg was obtained when starting from 1 mmol of CuCl. It is worthy to note that a second batch of 100 mg of CuNPs could be obtained from the supernatant with an average size of 7.1 nm ± 1.3 nm (18 % polydispersity, Figure 4b). These results are consistent with our initial expectations and validate the interest of this new access route to CuNPs.

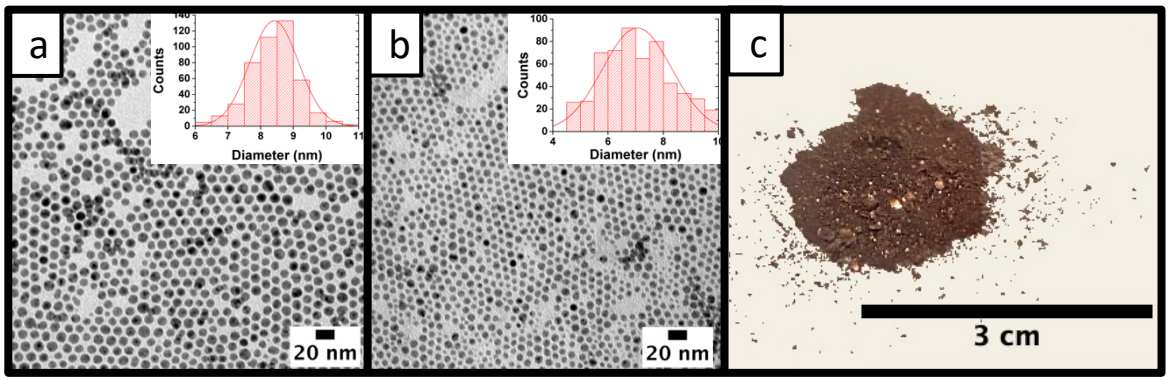

Figure 4. CuNPs prepared at the decigram scale. (a) Size histograms (in inset) and TEM images of the main batch of 270 mg (b) Size histograms (in inset) and TEM images of the 100 mg batch (c) picture of the main batch

3.6 Quantification of copper incorporation and estimated CuNPs yield from CuCl

As shown by the XPS analysis, the CuNPs surface is almost exclusively covered par thiols ligands (see section 3.3). Given that the surface coverage of NPs by thiols is estimated to 75%,[51] that dodecanethiol surface area is around 16 $Å^2$ and that the density of Cu is 8.9 $g.cm^{-3}$, it can be calculated from the results summarized in Table 3 that in the final NPs obtained in the optimized conditions (8 nm diameter of average size for the total CuNPs isolated from batch 1 and 2), the thiol ligands represent around 11% of their weight. This calculation of mass excess due to dodecanethiol ligands was validated by low frequency Raman spectroscopy measurements performed on silver nanoparticles.[52] However, we cannot exclude the presence of an excess of thiols trapped in the adsorbed thiols monolayer. It has been reported that the amount of trapped thiols is equal to the amount of adsorbed thiols according to infrared spectroscopy analysis of silver nanoparticles coated with thiols.[53] In order to calculate the most reliable yield we doubled the amount of thiols and in this case roughly 80% of NP weight thus corresponds to copper which means that the yield in the 5 mmol scale synthesis is almost quantitative, more than 90% of introduced copper being incorporated in overall isolated CuNPs (batch 1 + 2). It is worthy to note that the insoluble residue decanted away represents a very small amount as compared to the mass of salt introduced from the beginning. Moreover, the yield is not dependent on the scale, which shows the potential of the reported method in terms of scalability.

Table 3. Quantitative results and yield of CuNPs synthesis.

		Synthesis on 1 mmol scale	Synthesis on 5 mmol scale	
1	Size of the CuNPs	8.5 nm	8.4 nm	7.1 nm
2	Amount of Cu introduced at the beginning of the reaction (mg)	63	315	
3	Amount of thiol-stabilized CuNPs (mg)	50	270	100
4	Estimated yield of CuNPs (%)[a]	60	70	25

[a] Based on the characterization of the CuNPs surface and the estimated amount of DDT.[51-53]

3.7 Study of the reaction intermediates

A last set of experiments aimed at assessing the nature of the copper species formed before the addition of DDT. For this purpose, the reaction mixture was precipitated in the presence of ethanol after different reaction times and the precipitate was analysed by TEM (Figure 5).

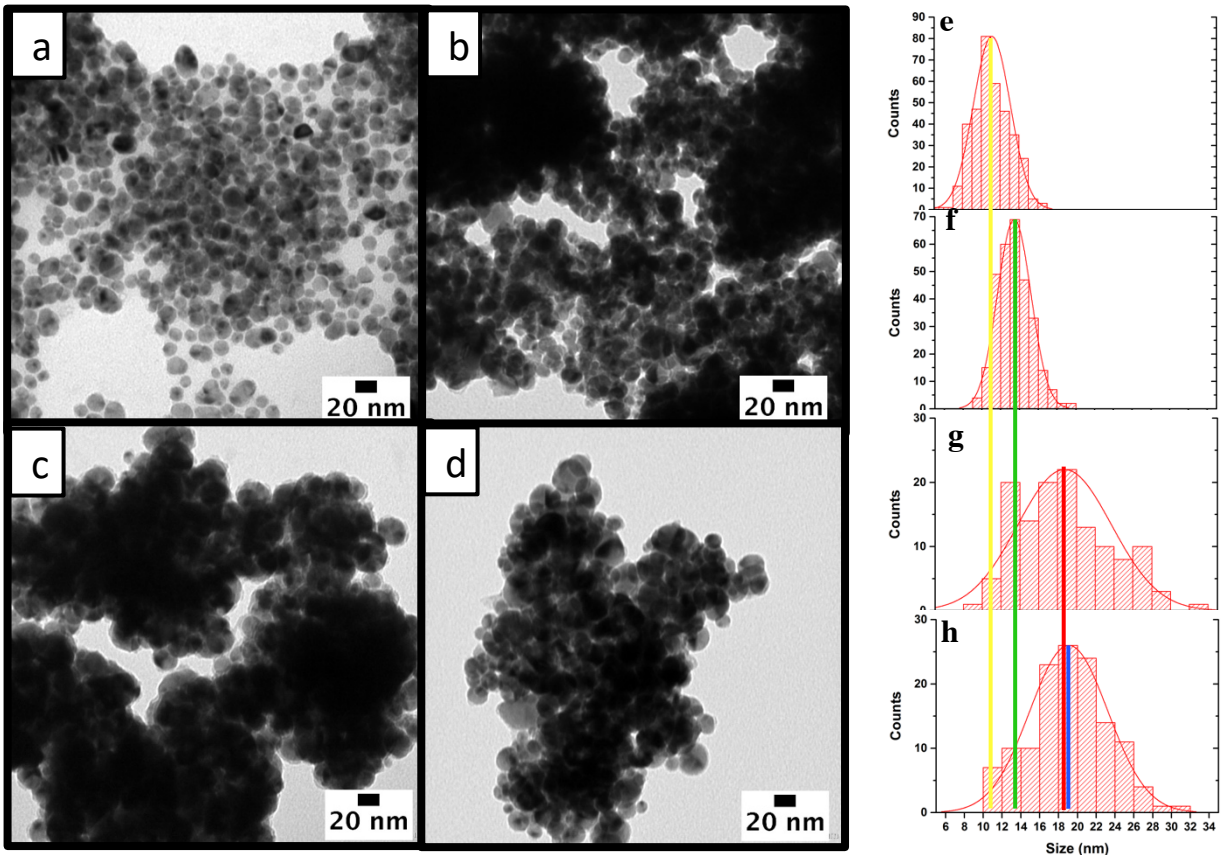

Figure 5. Representative TEM images of CuNPs obtained with different reaction times without addition of DDT at (a) 5 min (b) 10 min (c) 15 min and (d) 30 min and (e, f, g, h) the corresponding size histograms.

Interestingly, the TEM images showed a bulk phase likely composed of agglomerated quite polydisperse spheroid NPs. It is worthy to note that the size of these NPs was found to increase in the first 15 minutes from 11 (± 2) nm (18% polydispersity) after 5 minutes, to 13 (± 2) nm (15% polydispersity) after 10 minutes to finally reach a size of 19 (± 4) nm (20% polydispersity) after 15 or 30 minutes (Figures 4 (a)-(d)). Despite its moderate steric hindrance as compared to long-chain ligands usually employed in the preparation of CuNPs (Trioctylphosphine oxide (TOPO),

Trioctylphosphine (TOP), Oleylamine (OYA),[27-31] triphenylphosphine (PPh_3) seems to prevent the NP coalescence before the addition of DDT. The coordination of PPh_3 to CuNPs was already evidenced by IR spectroscopy.[33,34] Furthermore, PPh_3 have been widely used as ligands for gold and silver nanoparticles.[54] The ligand exchange reaction of PPh_3 stabilized CuNPs with dodecanethiols results in the rearrangement of the aggregates, leading to significantly smaller and dispersed NPs with well-defined spherical morphologies. A study carried out by Woehrle et al. on gold NPs coated with PPh_3 showed a similar phenomenon of digestive ripening during the exchange of phosphine ligands by thiols with the loss of gold core atoms and a decrease in the size of the NPs.[55-56] A surface etching of particles may be followed by the subsequent growth of the remaining ones through the re-deposition of the etched species process.[57] This phenomenon that implies a rearrangement at the atomic scale may rationalize the transformation of the transient large spheroids into smaller NPs with low loss of copper matter. Remarkably, the conditions operating here are very mild as compared to usual processes implying higher temperatures, as for example in the case of CuNPs (toluene reflux 110 °C).[58] Furthermore, the final size of the NPs could be controlled by the amount of DDT added. Decreasing the amount of DDT from 4 to 2 equivalents induced an increase of the NPs size and polydispersity from 8.5 ± 0.4 nm to 14 ± 4 nm (Figures 1c and 5a, respectively). On the contrary, the use of 8 equivalents of DDT yielded slightly smaller NPs of 6.2 ± 0.5 nm size with a low size dispersity (Figure 5b). This last result is particularly attractive since tuning the size of NPs is of crucial interest for many applications and for example as far as catalysis is concerned.[59]

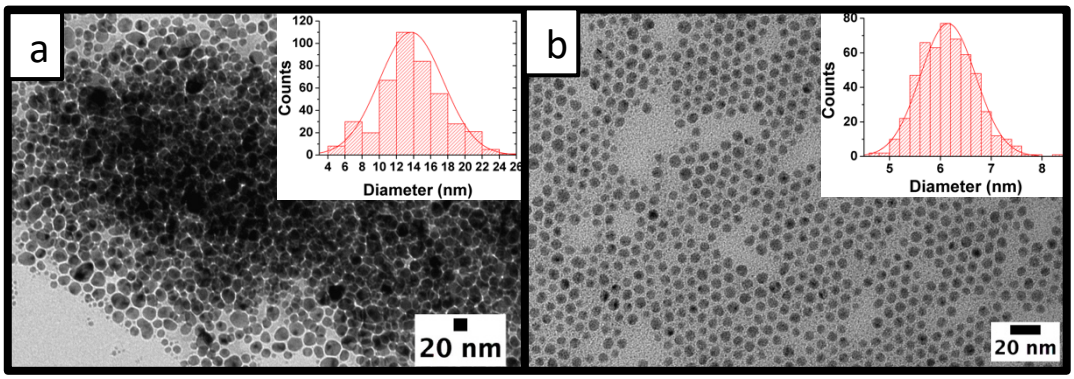

Figure 5. Size histograms (in inset) and TEM images of CuNPs prepared from CuCl, PPh_3 (5 equiv), *n*-BuMgCl in refluxing THF and stabilized by different amounts of DDT: (a) 2 equiv. (as compared to copper) and (b) 8 equiv.

4 Conclusion

In summary, we report an innovative and robust synthetic method for the fast preparation of spherical CuNPs with controlled size and shape. The main advantages are i) the very mild conditions used and the easy implementation of the synthesis (no gas under pressure, low temperature); ii) the few additives required; iii) the low cost and availability of the starting reagents; iv) the time-saving procedure and v) the possibility to obtain the CuNPs on a decigram scale. The full potential of this new synthesis way to metallic nanoparticles is currently under study in our laboratories. Besides, the possibility of finely controlling the size of the prepared CuNPs it is noteworthy that ligands cover partially the surface and that there is "naked" reactive metallic sites available. It makes them particularly attractive for applications in homogeneous, electrochemical and plasmonic catalysis. In particular, we believe that in the future we will be able to gain a thorough understanding of the mechanism of plasmon-assisted reactions and move

towards the large-scale industrial application of these copper-based plasmonic catalysts due to the high efficiency of our syntheses.

ASSOCIATED CONTENT

Supporting Information. The following files are available free of charge.

Experimental details of CuNPs synthesis with evolving reaction conditions, material characterizations and additional figures (PDF file).

AUTHOR INFORMATION

Corresponding Author

*Pr Alexa Courty: alexa.courty@sorbonne-universite.fr; *Dr Armelle Ouali: armelle.ouali@enscm.fr; *Dr Emmanuel Vrancken: emmanuel.vrancken@enscm.fr

Author Contributions

The manuscript was written through contributions of all authors. All authors have given approval to the final version of the manuscript.

ACKNOWLEDGMENT

The authors thank the Ecole Nationale de Chimie de Montpellier (ENSCM) for the thesis grant, LO, AO and EV thank ENSCM, UM and the CNRS for facilities.

REFERENCES

[1] Chanderiya, G.; Naikoo, A.; Das, R.; Hassan, I. U.; Kashaw, S. K.; Pandey, S. Recent Advances in Metal Nanoparticles for the Synthesis of N-Containing Heterocyclic Compounds: A Mini Review. *Asian J. Chem.* **2021**, *33*, 949-955.

[2] Axet, M. R.; Philippot, K. Catalysis with Colloidal Ruthenium Nanoparticles. *Chem. Rev.* **2020**, *120*, 1085-1145.

[3] Rai, P. Plasmonic Noble Metal@Metal Oxide Core–Shell Nanoparticles for Dye-Sensitized Solar Cell Applications. *Sustainable Energy Fuels*, **2019**, *3*, 63-91.

[4] Stewart, S.; Wei, Q.; Sun, Y. Surface Chemistry of Quantum-Sized Metal Nanoparticles under Light Illumination. *Chem. Sci.*, **2021**, *12*, 1227-1239.

[5] Oyarzun, M. P.; Tapia-Arellano, A.; Cabrera, P.; Jara-Guajardo, P.; Kogan, M. J. Plasmonic Nanoparticles as Optical Sensing Probes for the Detection of Alzheimer's Disease. *Sensors*, **2021**, *21*, 2067.

[6] Montes-Garcia, V.; Squillaci, M. A.; Diez-Castellnou, M.; Khac Ong, Q.; Stellacci, F.; Samori, P. Chemical Sensing with Au and Ag Nanoparticles. *Chem. Soc. Rev.*, **2021**, *50*, 1269-1304.

[7] Xu, N.; Jin, S.; Wang, L. Metal Nanoparticles-based Nanoplatforms for Colorimetric Sensing: A review. *Reviews in Analytical Chemistry*, **2021**, *40*, 1-11.

[8] Azharuddin, M.; Zhu, G. H.; Das, D.; Ozgur, E.; Uzun, L.; Turner, A. P. F.; Patra, H. K. A repertoire of Biomedical Applications of Noble Metal Nanoparticles. *Chem. Commun.* **2019**, *55*, 6964-6996.

[9] Krajczewski, J.; Rucinska, K.; Townley, H. E.; Kuderski, A. Role of various Nanoparticles in Photodynamic Therapy and Detection Methods of Singlet Oxygen *Photodiagnosis and Photodynamic Therapy*, **2019**, *26*, 162-178.

[10] Barui, A. K.; Kotcherlakota, T.; Patra, C. R. In *Metal Nanoparticles: Synthesis and Applications in Pharmaceutical* Sciences. Thota, S.; Debbie C. Crans, D. C., Eds; Wiley-VCH Verlag GmbH & Co. KGaA, Weinheim, Germany 2018; pp 121-153.

[11] Heuer-Jungemann, A.; Feliu, N.; Bakaimi, I.; Hamaly, M.; Alkilany, A.; Chakraborty, I.; Masood, A.; Casula, M. F.; Kostopoulou, A.; Oh, E. et al. The Role of Ligands in the Chemical Synthesis and Applications of Inorganic Nanoparticles. *Chem. Rev.* **2019**, *119*, 4819-4880.

[12] Amiens, C. ; Chaudret, B. ; Ciuculescu-Pradines, D. ; Collière, V. ; Fajerwerg, K. ; Fau, P. ; Kahn, M. ; Maisonnat, A.; Soulantica, K.; Philippot, K. Organometallic Approach for the Synthesis of Nanostructures. *New. J. Chem.*, **2013**, *37*, 3374-3401.

[13] Zao, S.; Han, F.; Li, J.; Meng, X.; Huang, W.; Cao, D.; Zhang, G.; Sun, R.; Wang, C.-P. Advancements in Copper Nanowires: Synthesis, Purification, Assemblies, Surface Modification, and Applications. *Small* **2018**, *14*, 1800047.

[14] Shah, K. W.; Lu, Y. Morphology, large scale Synthesis and Building Applications of Copper Nanomaterials. *Construction and Building Materials* **2018**, *180*, 544-578.

[15] Gawande, M. B.; Goswami, A.; Felpin, F.-X.; Asefa, T.; Huang, X.; Silva, R.; Zou, X.; Zboril, R.; Varma, R. S. Cu and Cu-Based Nanoparticles: Synthesis and Applications in Catalysis. *Chem. Rev.* **2016**, *116*, 3722-3811.

[16] Qing, Z.; Bai, A.; Xing, S.; Zou, Z.; He, X.; Wang, K.; Yang, R. Progress in Biosensor Based on DNA-templated Copper Nanoparticles. *Biosens Bioelectron*. **2019**, *137*, 96-109.

[17] Rifat, A. A.; Mahdiraji, G. A.; Ahmed, R.; Chow, D. M.; Sua, Y. M.; Shee, Y. G.; Adikan, F. R. M. Copper-Graphene-Based Photonic Crystal Fiber Plasmonic Biosensor. *IEEE Photonics J*. **2016**, *8*, 4800408.

[18] Chapus, L.; Aubertin, P.; Joiret, S. ; Lucas, I. T. ; Maisonhaute, E.; Courty, A. Tunable SERS Platforms from Small Nanoparticle 3D Superlattices: A Comparison between Gold, Silver, and Copper. *ChemPhysChem* **2017**, *18*, 3066-3075.

[19] Böhme, A.; Sterl, F.; Kath, E.; Ubl, M.; Manninen, V.; Giessen, H. Electrochemistry on Inverse Copper Nanoantennas: Active Plasmonic Devices with Extraordinarily Large Resonance Shift *ACS Photonics* **2019**, *6,* 1863-1868.

[20] Chan, G. H.; Zhao, J.; Hicks, E. M.; Schatz, G. C.; Van Duyne R. P. Plasmonic Properties of Copper Nanoparticles Fabricated by Nanosphere Lithography *Nano Lett*. **2007**, *7*, 1947-1952.

[21] Karelovic, A.; Galdames, G.; Medina, J. C.; Yévenes, C.; Barra, Y.; Jiménez, R. Mechanism and Structure Sensitivity of Methanol Synthesis from CO_2 over SiO_2-Supported Cu Nanoparticles. *J. Catal*. **2019**, *369*, 415-426.

[22] Noh, G.; Docherty, S. R., Lam, E.; Huang, X.; Mance, D.; Altke, J. L.; Copéret, C. CO_2 Hydrogenation to CH_3OH on Supported Cu Nanoparticles: Nature and Role of Ti in Bulk Oxides vs Isolated Surface Sites. *J. Phys. Chem. C* **2019**, *123*, 31082-31093.

[23] Dongare, S.; Singh, N.; Bhunia, H., Electrocatalytic reduction of CO_2 to useful chemicals on copper nanoparticles. *Applied Surface Science* **2021**, *537*, 148020.

[24] Kim, S.; Jae-Myoung Kim, J.-M.; Jeong-Eun Park, J.-E.; Nam, J.-M. Nonnoble-Metal-Based Plasmonic Nanomaterials: Recent Advances and Future Perspectives. *Adv. Mater.* **2018**, *30*, 1704528.

[25] Wang, D.; Astruc, D. The Recent Development of Efficient Earth-Abundant Transition-Metal Nanocatalysts. *Chem. Soc. Rev.* **2017**, *46*, 816-854.

[26] Singer, R. A.; Monfette, S.; Bernhardson, D. J.; Tcyrulnikov, S.; Hansen, E. C. Recent Advances in Nonprecious Metal Catalysis. *Org. Process Res. Dev.* **2020**, *24*, 909-915.

[27] Strach, M.; Mantella, V.; Pankhurst, J. R.; Iyengar, P.; Loiudice, A.; Das, S.; Corminboeuf, C.; van Beek, W.; Buonsanti, R. Insights into Reaction Intermediates to Predict Synthetic Pathways for Shape-Controlled Metal Nanocrystals. *J. Am. Chem. Soc.* **2019**, *141*, 16312-16322.

[28] Yang, H.-J.; He, S.-Y.; Chen, H.-L.; Tuan, H.-Y. Monodisperse Copper Nanocubes: Synthesis, Self-Assembly, and Large-Area Dense-Packed Films. *Chem. Mater.* **2014**, *26*, 1785-1793.

[29] Guo, H.; Chen, Y.; Cortie, M. B.; Liu, X.; Xie, Q.; Wang, X.; Peng, D.-L. Shape-Selective Formation of Monodisperse Copper Nanospheres and Nanocubes via Disproportionation Reaction Route and Their Optical Properties. *J. Phys. Chem. C* **2014**, *118*, 9801-9808.

[30] Guo, H.; Liu, X.; Xie, Q.; Wang, L.; Peng, D.-L.; Branco, P. S.; Gawande, M. B. Disproportionation Route to Monodispersed Copper Nanoparticles for the Catalytic Synthesis of Propargylamines. *RSC Adv.* **2013**, *3*, 19812-19815.

[31] Ye, E.; Zhang, S.-Y.; Liu, S.; Han, M.-Y. Disproportionation for Growing Copper Nanowires and their Controlled Self-Assembly Facilitated by Ligand Exchange. *Chem. Eur. J.* **2011**, *17*, 3074-3077.

[32] Barrière, C.; Piettre, K.; Latour, V.; Margeat, O.; Turrin, C.-O.; Chaudret, B.; Fau, P. Ligand Effects on the Air Stability of Copper Nanoparticles obtained from Organometallic Synthesis. *J. Mater. Chem.* **2012**, *22*, 2279-2285.

[33] Ali Ben Aissa, M.; Tremblay, B.; Andrieux-Ledier, A.; Maisonhaute, E.; Raouafi, N.; Courty, A. Copper Nanoparticles of well-controlled Size and Shape: a new Advance in Synthesis and Self-Organization. *Nanoscale* **2015**, *7*, 3189-3195.

[34] Frogneux, X.; Hippolyte, L.; Mercier, D.; Portehault, D.; Chanéac, C.; Sanchez, C.; Marcus, P.; Ribot, F.; Fensterbank, L.; Carenco, S. Direct Synthesis of N-Heterocyclic Carbene-Stabilized Copper Nanoparticles from an N-Heterocyclic Carbene–Borane. *Chem. Eur. J.* **2019**, *25*, 11481-11485.

[35] Frogneux, X.; Borondics, F.; Lefrançois, S.; D'Accriscio, F.; Sanchez, C.; Carenco, S. Surprisingly High Sensitivity of Copper Nanoparticles toward Coordinating Ligands: Consequences for the Hydride Reduction of Benzaldehyde. *Catal. Sci. Technol.* **2018**, *8*, 5073-5080.

[36] Saikova, S. V.; Vorob'ev, S. A.; Nikolaeva, R. B.; Mikhlin, Y. L. Conditions for the Formation of Copper Nanoparticles by Reduction of Copper(II) Ions with Hydrazine Hydrate Solutions. *Russ. J. Gen. Chem.* **2010**, *80*, 1122-1127.

[37] *The Chemistry of Organocopper Compounds*; Rappoport, Z.; Marek, I., Eds.; Wiley, London, 2009.

[38] *Modern Organocopper Chemistry*; Krause, N., Ed.; Wiley—VCH, Mörlenbach, 2002.

[39] Vrancken E.; Campagne J.-M.; Mangeney P. In: *Comprehensive Organic Synthesis*, Molander, G. A.; Knochel, P., Eds.; 2nd edition, Vol 1; Oxford: Elsevier; 2014, pp. 74-123.

[40] Ouali, A.; Taillefer, M. Grignard Reagents and Copper. *Phys. Sci. Rev.* **2016**, *1*, 20160037.

[41] Whitesides, G. M.; Stedronsky, E. R.; Casey, C. P.; San Filippo Jr, J. Mechanism of Thermal Decomposition of *n*-butyl(tri-*n*-butylphosphine) Copper(I). *J. Am. Chem. Soc.* **1970**, *92*, 1426-1427.

[42] Wada, K.; Tamura, M.; Kochi, J. Autocatalytic Decomposition of Alkylcopper(I) Species. Electron Spin Resonance Spectrum of Binuclear Copper(0) Intermediates. *J. Am. Chem. Soc.* **1970**, *92*, 6656-6658.

[43] Miyashita, A.; Yamamoto, T.; Yamamoto, A. Thermal Stability of Alkylcopper(I) Complexes Coordinated with Tertiary Phosphines. *Bull. Soc. Chem. Jpn* **1977**, *50*, 1109-1117.

[44] Pasynkiewicz, S. Thermal decomposition of nickel-carbon and copper-carbon σ-bonds. *J. Organomet. Chem.* **190**, *387*, 1-10.

[45] Pasynkiewicz, S.; Pikul, S.; Poplawska, J. Synthesis and Thermal Decomposition of methyl(tri-*t*-butylphosphine)copper. *J. Organomet. Chem.* **1985**, *293*, 125-130.

[46] Lee, S.; Portalès, H.; Walls, M.; Beaunier, P.; Goubet, N.; Tremblay, B.; Margueritat, J.; Saviot, L.; Courty, A. Versatile and Robust Synthesis Process for the Fine Control of the Chemical Composition and Core-Crystallinity of Spherical Core–Shell Au@Ag Nanoparticles. *Nanotechnology* **2020**, *32*, 095604.

[47] Laibinis, P. E.; Whitesides, G. M. Self-assembled Monolayers of *n*-alkanethiolates on Copper are Barrier Films that Protect the Metal against Oxidation by Air. *J. Am. Chem. Soc.* **1992**, *114*, 9022-9028.

[48] Castner, D. G.; Hinds, K.; Grainger, D. W. X-ray Photoelectron Spectroscopy Sulfur 2p Study of Organic Thiol and Disulfide Binding Interactions with Gold Surfaces. *Langmuir* **1996**, *12*, 5083-5086.

[49] S.-m. Chang, Y.-y. Hsu, T.-s. Chan, Chemical Capture of Phosphine by a Sol–Gel-Derived Cu/TiO_2 Adsorbent – Interaction Mechanisms. *J. Phys. Chem. C* **2011**, *115*, 2005-2013.

[50] Tahir, D.; Tougaard, S. Electronic and Optical Properties of Cu, CuO and Cu_2O Studied by Electron Spectroscopy. *J. Phys.: Condens. Matter* **2012**, *24*, 175002.

[51] Korgel, A.; Fullan, S.; Connelly, S.; Fitzmaurice, D. Assembly and Self-Organization of Silver Nanocrystal Superlattices: Ordered "Soft Spheres. *J. Phys. Chem. B* **1998**, *102*, 8379-8388.

[52] Courty, A.; Lisiecki, I.; Pileni, P. Vibration of Self-organized Silver Nanocrystals. *J. Chem. Phys.* **2002**, *116*, 8074-8078.

[53] Andrieux-Ledier, A.; Tremblay B.; Courty, A. Stability of Self-Ordered Thiol-Coated Silver Nanoparticles: Oxidative Environment Effects. *Langmuir* **2013**, *29*, 13140–13145.

[54] Andrieux-Ledier, A.; Tremblay B.; Courty, A. Synthesis of Silver Nanoparticles Using Different Silver Phosphine Precursors: Formation Mechanism and Size Control. *J. Phys. Chem. C* **2013**, *117*, 14850–14857.

[55] Woehrle, G. H.; Brown, L. O.; Hutchinson, J. E. Thiol-Functionalized, 1.5-nm Gold Nanoparticles through Ligand Exchange Reactions: Scope and Mechanism of Ligand Exchange. *J. Am. Chem. Soc.* **2005**, *127*, 2172-2183.

[56] Woehrle, G. H.; Hutchinson, J. E. Thiol-Functionalized Undecagold Clusters by Ligand Exchange: Synthesis, Mechanism, and Properties. *Inorg. Chem.* **2005**, *44*, 6149-6158.

[57] Shimpi, J. R.; Sidhaye, D. S.; Parsad, B. L. V. Digestive Ripening: A Fine Chemical Machining Process on the Nanoscale. *Langmuir* **2017**, *33*, 9491-9507.

[58] Shaik, A. H.; Chakraborty, J. Synthesis of Monodisperse Copper Nanoparticles Using a Modified Digestive Ripening Technique and Formation of Superlattices. *RSC Adv.* **2015**, *5*, 85974-85977.

[59] Karelovic, A.; Ruiz, P. The Role of Copper Nanoparticle Size in Low Pressure Methanol Synthesis via CO_2 Hydrogenation over Cu/ZnO Catalysts. *Catal. Sci. Technol.* **2015**, *5*, 869-881.

SYNOPSIS

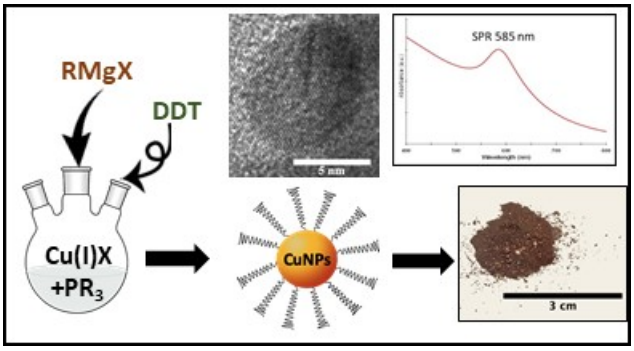

Supporting Information

Copper Nanoparticles with Tunable Size: Implications for Plasmonic Catalysis

Liyan Ouyang,[a] *Vincent* Noël,[b] *Alexa Courty,*[*c] *Jean-Marc Campagne,*[a] *Armelle Ouali,*[*a] *and Emmanuel Vrancken*[*a]

[a] Institut Charles Gerhardt Montpellier, Univ. Montpellier, CNRS, ENSCM, Montpellier, France.

[b] Université de Paris, ITODYS, CNRS, F-75006 Paris, France

[c] Sorbonne Université, MONARIS, UMR8233, 75005 Paris, France.

E-mail: alexa.courty@sorbonne.universite.fr; armelle.ouali@enscm.fr; emmanuel.vrancken@enscm.fr,

1. Experimental

Chemicals and instrumentations

Commercial reagents were used without further purification, except stated otherwise, and stored in a glovebox in order to avoid any traces of moisture or air contamination. The following chemicals were purchased from SIGMA: copper (I) chloride (99.99 %), Butylmagnesium chloride solution (*n*-BuMgCl, 2.0 M solution in THF), triphenylphosphine (99 %), 1-dodecanethiol (≥ 98 %). Hexane, chloroform and absolute ethanol were purchased from SIGMA, VWR and CARLO ERBA. THF was distilled over sodium/benzophenone and handled under an atmosphere of nitrogen.

Transmission electron microscopy (TEM). TEM images of copper nanoparticles (CuNPs) were obtained using a JOEL 1200 EX microscope with an accelerating voltage of 120kV. All CuNPs samples were prepared by dropping the nanoparticles suspensions in hexane or chloroform onto a carbon-coated nickel grid, then dried on the surface of the grid under inert gas. For each sample, TEM images were taken from different parts of the grid and used to estimate size distribution of copper nanoparticles. High-resolution TEM (HRTEM) images and selected area electron diffraction (SAED) patterns were collected on a JOEL 2200FS TEM at 200KV. Image J software was used for measuring the size of nanoparticles around 300-500 NPs and the size distribution was determined using the Origin-Pro 9.1.

Ultraviolet-visible (UV-Vis) Spectroscopy. The UV-Vis spectroscopy was performed on a V-770 UV-Visible/NIR spectrophotometer at room temperature with the wavelength range of 300 to 800 nm. Before each run, background subtraction was performed with the solvent system of choice. The measurements were performed in a quartz cell with 1cm optical path length.

X-ray photoelectron spectroscopy (**XPS**) was conducted with a K-Alpha+ system (ThermoFisher Scientific, East-Grinsted, UK) fitted with a micro-focused and monochromatic Al Kα X-ray source (spot size of 400 μm, 1486.6 eV). Spectrometer pass energy was 150 eV for the survey and 40 eV for the narrow high-resolution regions. The samples were prepared by depositing several drops of the solution on a silicon wafer. TEM images were recorded prior to XPS analysis to ensure that individual nanoclusters are actually present. In this study, the surface characterization of elements of Cu, P, S, Mg, C, and Cl of CuNPs was performed.

Podwer X-Ray Diffraction (XRD). Powder XRD pattern were collected with Ni-filtered Cu $K_{\alpha 1/\alpha 2}$ (λ = 1.5418Å) radiation in a reflection geometry on a Pananalytical X'Pert Pro-MPD diffractometer, operating at a working voltage and current of 45 KV and 20 mA. In preparing the sample, the powder sample was formed by precipitating of nanoparticles with ethanol and centrifuging at 4000 rpm for 10min before drying at room temperature in an N_2-filled glovebox. The dry precipitate was pulverized and the resulting powder was used to fill a glass plate.

Synthesis of copper nanoparticles (CuNPs).

CuNPs prepared in the presence of 1-5 equiv. of PPh_3 at 25 °C

CuCl (99 mg, 1 mmol, 1 equiv.) and PPh_3 [1 equiv. (262 mg, 1 mmol), or 3 equiv. (787 mg, 3 mmol), or 5 equiv. (31 g, 5 mmol)] were dissolved in 10 mL of dry THF in a 25 mL flask inside a nitrogen filled glovebox by strong magnetic stirring at room temperature. After all the solids were dissolved and colorless solution obtained, *n*-BuMgCl (2.0 M solution in THF, 1 equiv., 0.5 mL, 1 mmol) was quickly injected into the colorless solution. The color of the suspension gradually changed from colorless to yellow, bright orange and finally dark with varied intermediate stages. After 15 min, 1-dodecanethiol (4 equiv., 1 mL, 4 mmol) was added and the reaction medium consequently turned to dark-red. After 1h of stirring at room temperature, the reaction was stopped. The copper nanoparticles were precipitated by centrifugation of the mix at 2500 rpm for 10 min. The supernatants were decanted away and chloroform was added to the precipitate, the nanoparticles with varied sizes were separated by centrifugation at 4000 rpm for 5 min. After two dissolution-precipitation cycles, the Cu nanospheres were dispersed in anhydrous hexane and dropped on TEM grid for further analysis.

Note: With 5 equiv. PPh_3, the formation of a gel was observed, preventing the stirring of the solution and thus the formation of well-defined CuNPs.

CuNPs prepared in the presence of 1-5 equiv. of PPh_3 at 65 °C

CuCl (1 equiv., 99 mg, 1 mmol) and PPh_3 [1 equiv. (262 mg, 1 mmol), or 3 equiv. (787 mg, 3 mmol), or 5 equiv. (1.31 g, 5 mmol)] were dissolved in 10 mL of dry THF in a 25 mL three-neck flask connected to a Schlenk line was purged under nitrogen by strong magnetic stirring at 65°C. After all the solids were dissolved and colorless solution obtained, *n*-BuMgCl (2.0 M solution in THF, 1 equiv., 0.5 mL, 1 mmol) was quickly injected into the colorless solution with a syringe. The color of suspension gradually changed from colorless, bright-yellow and finally dark. After 15 min (or 30 s, or 5 min, or 30 min) of heating at 65°C, 1-dodecanethiol (4 equiv.,

1 mL, 4 mmol.) was added into the mixture and a dark-red suspension was obtained. The reaction was stirred at 65°C for 1h before cooling to room temperature. The copper nanoparticle suspension was centrifuged directly at 2500 rpm for 10 min. Then the precipitate was decanted away and absolute ethanol was added to the red supernatant, Cu nanospheres were precipitated by centrifugation at 4000 rpm for 5 min. They were dispersed in anhydrous chloroform and collected by centrifugation at 4000 rpm for 5 min, the Cu nanospheres were dropped on a TEM grid for further analysis.

CuNPs prepared in the presence of 5 equiv. of PPh_3 at 65 °C without addition of DDT.
CuCl (1 equiv., 99 mg, 1 mmol) and PPh_3 (5 equiv., 1.31 g, 5 mmol) were dissolved in 10 mL of dry THF in a 25 mL three-neck flask connected to a Schlenk line was purged under nitrogen by strong magnetic stirring at 65°C. After all solids were dissolved and colorless solution obtained, *n*-BuMgCl (2.0 M solution in THF, 1 equiv., 0.5 mL, 1 mmol) was quickly injected into the colorless solution of copper salt using a syringe. The color of the reaction medium gradually changed from colorless to bright-yellow and finally dark. The reaction was next stirred at 65°C for 5 min (or 15 min, or 30 min) before cooling to room temperature. The copper nanoparticles were precipitated by centrifugation at 2500 rpm for 10 min. The supernatants were decanted away and the precipitate subsequently dissolved in chloroform followed by centrifugation at 4000 rpm for 5 min. After two dissolution-precipitation cycles, the Cu nanoparticles were dispersed in anhydrous hexane and dropped on TEM grid for further analysis.

2. CuNPs prepared in the presence of 3 or 5 equiv. of PPh_3 at 25 °C or 65 °C.

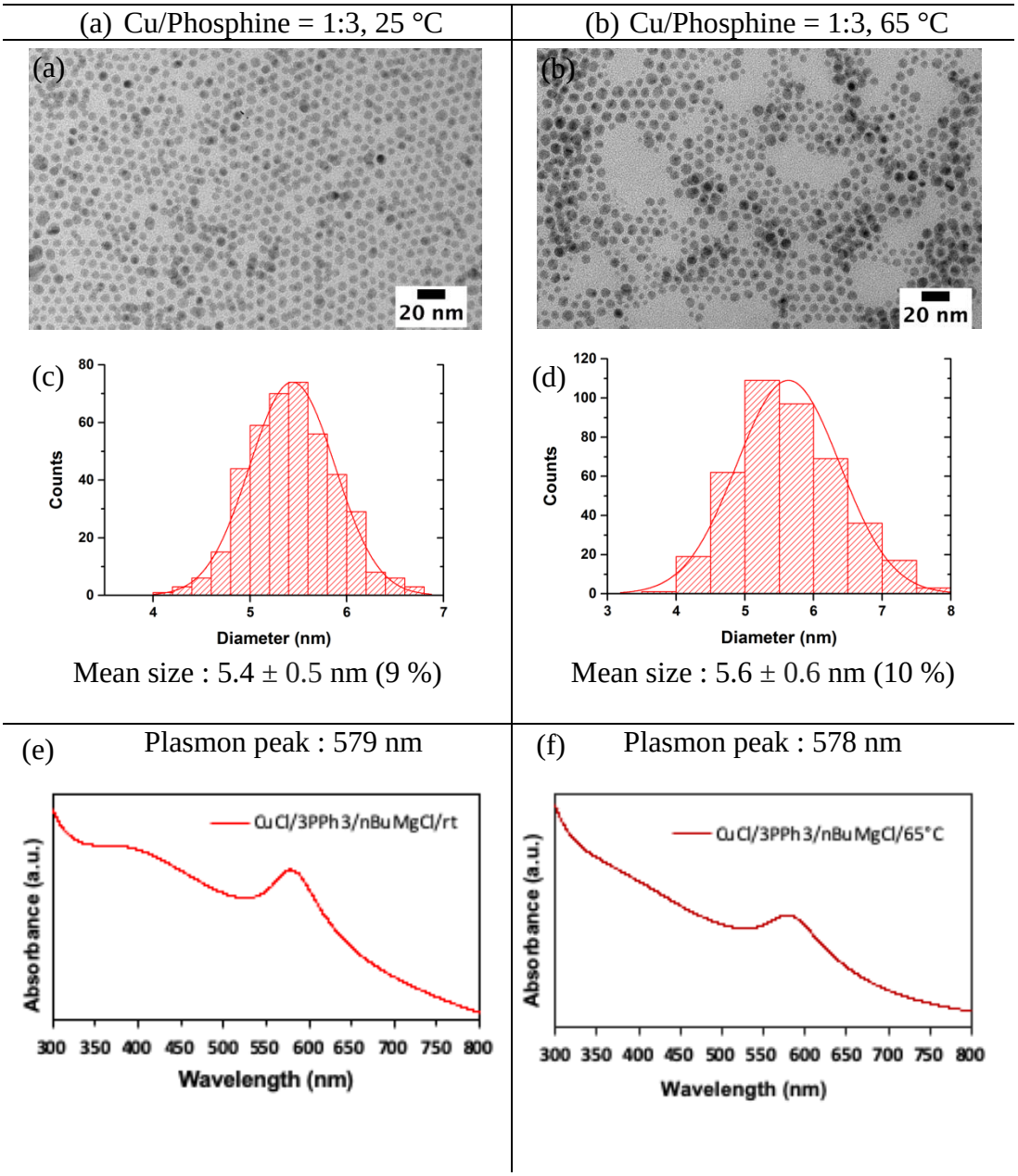

Figure S1: (a-d) TEM images and corresponding size histograms of the CuNPs prepared in the presence of 3 equiv. of PPh_3 at 25°C and 65 °C. (e, f) the corresponding UV-Vis spectra.

3. CuNPs prepared in the presence of 1 equiv. of PPh_3 at 25 °C or 65 °C.

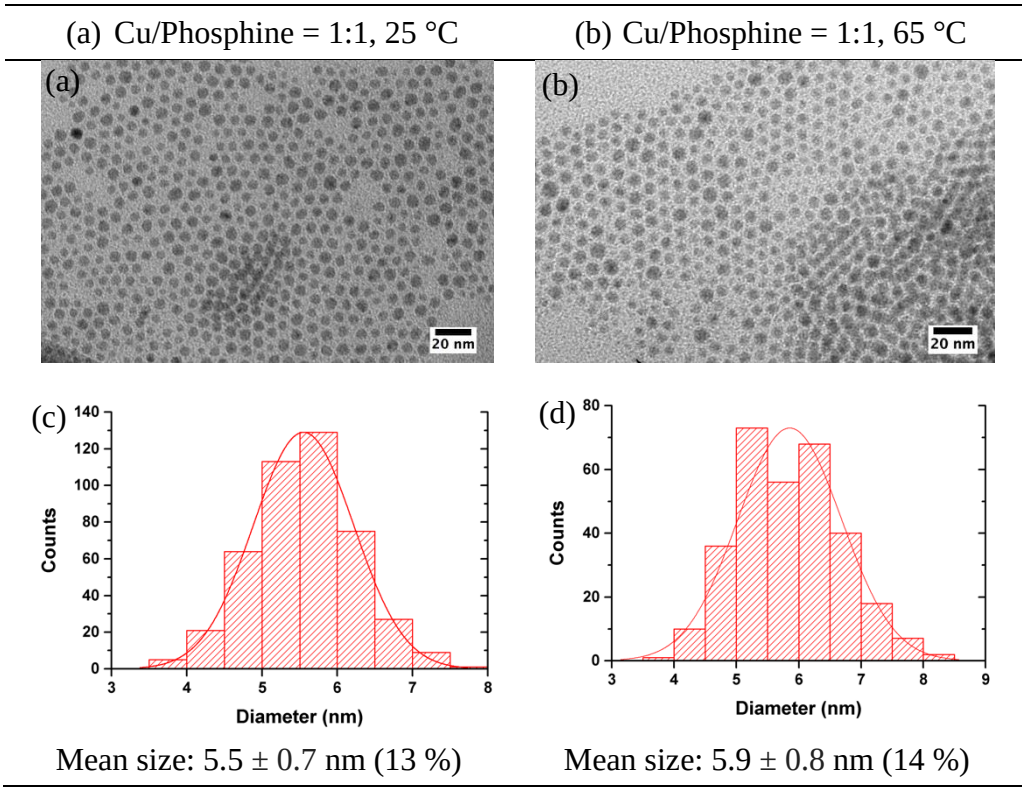

Figure S2: (a-d) TEM images and corresponding size histograms of the NPs prepared with a copper-to-PPh_3 ratio of 1:1 at 25°C and 65°C

4. CuNPs prepared in the presence of 5 equiv. of PPh_3 at 65 °C with varied addition times of DDT.

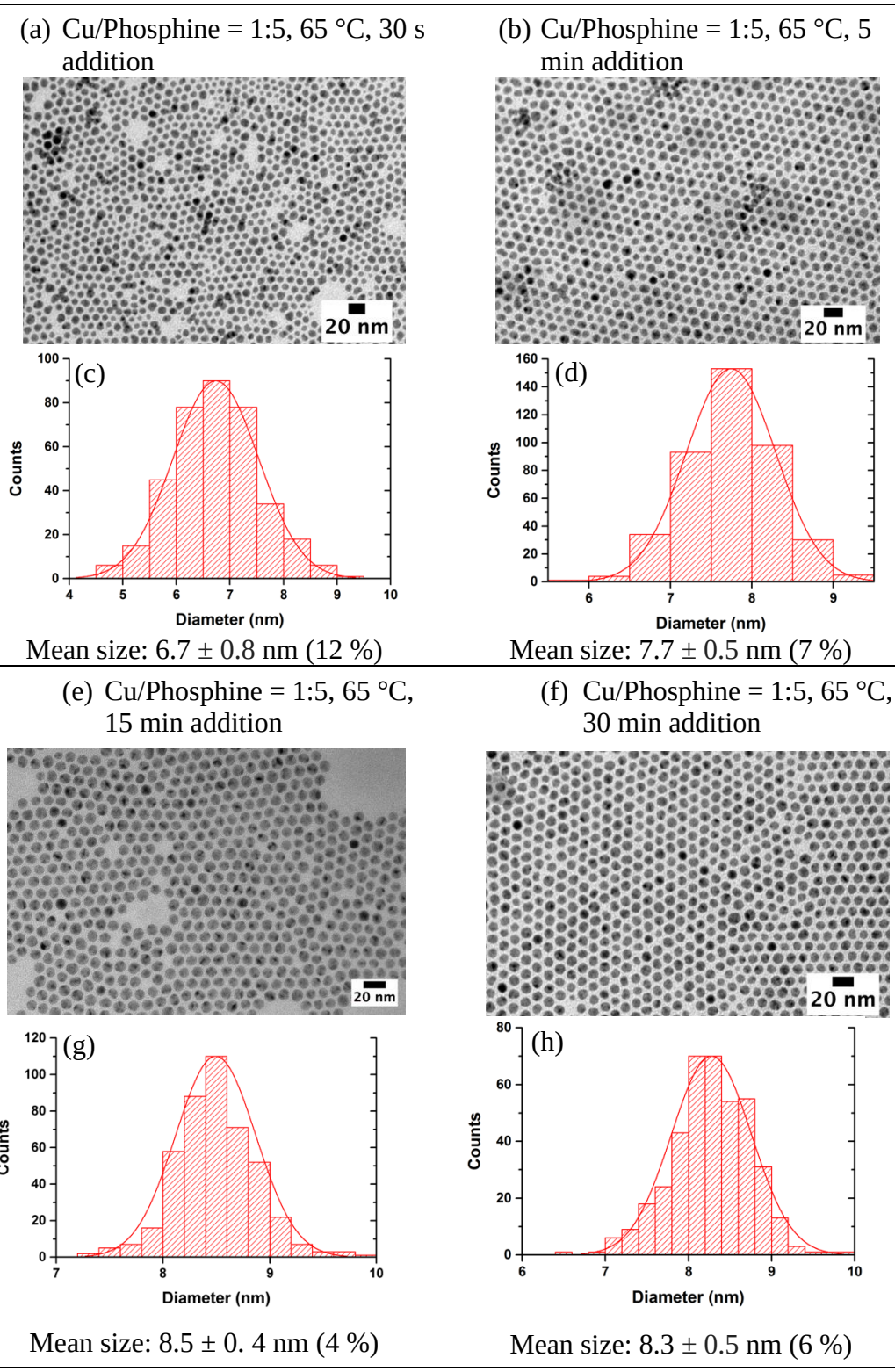

Figure S3: TEM images of the NPs prepared with a copper-to-PPh_3 ratio of 1:5 at 65°C with varied addition times of DDT (4 equiv.) (a) 30s (b) 5 min (c) 15 min (d) 30 min.

5. HRTEM of CuNPs prepared in the presence of 5 equiv. of PPh_3 at 65 °C.

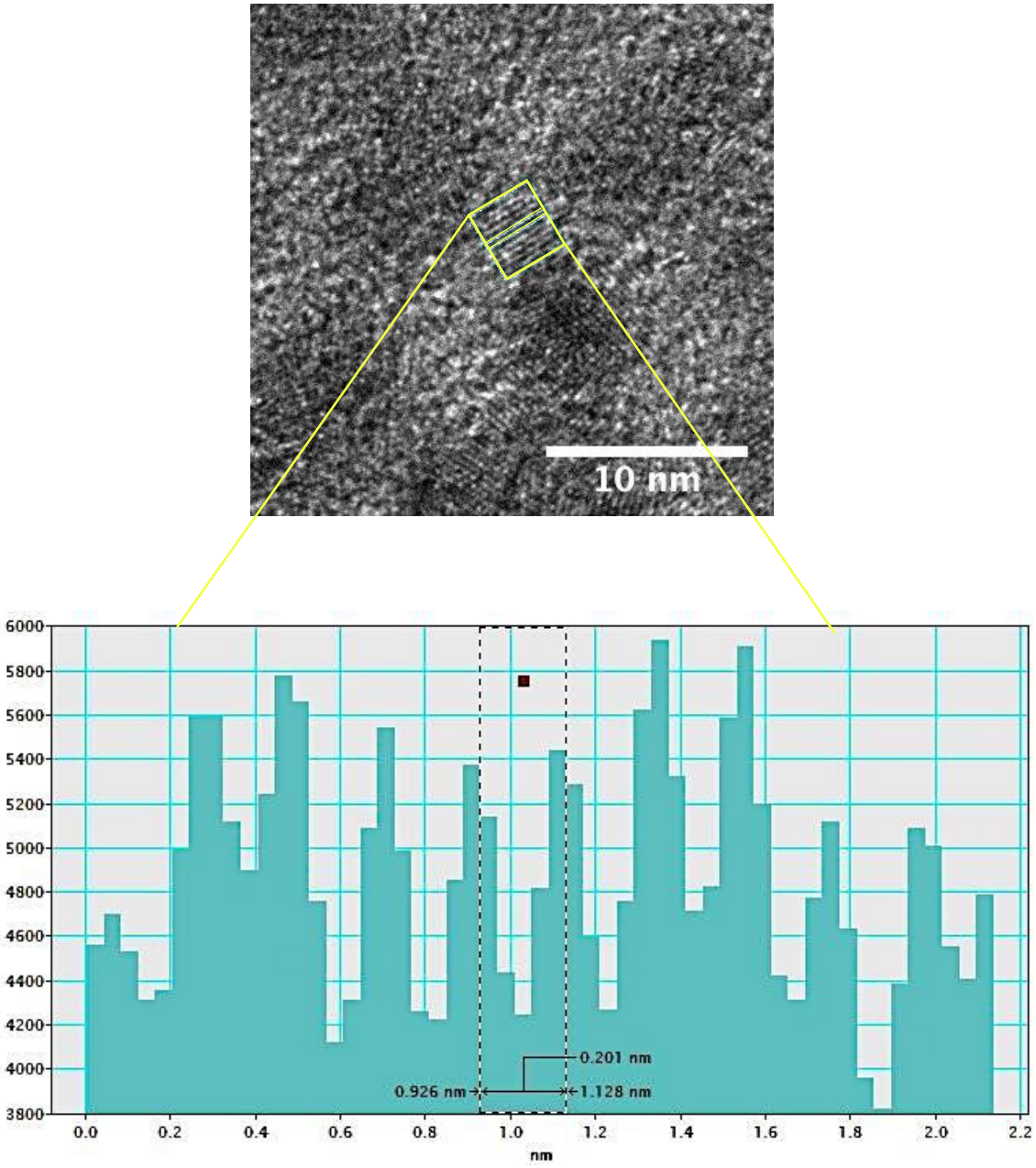

Figure S4. The $d_{\text{-spacing}}$ analysis from HRTEM image of a single Cu nanosphere.

6. X-ray photoelectron spectroscopy (XPS) of CuNPs prepared in the presence of 5 equiv. of PPh_3 at 65 °C.

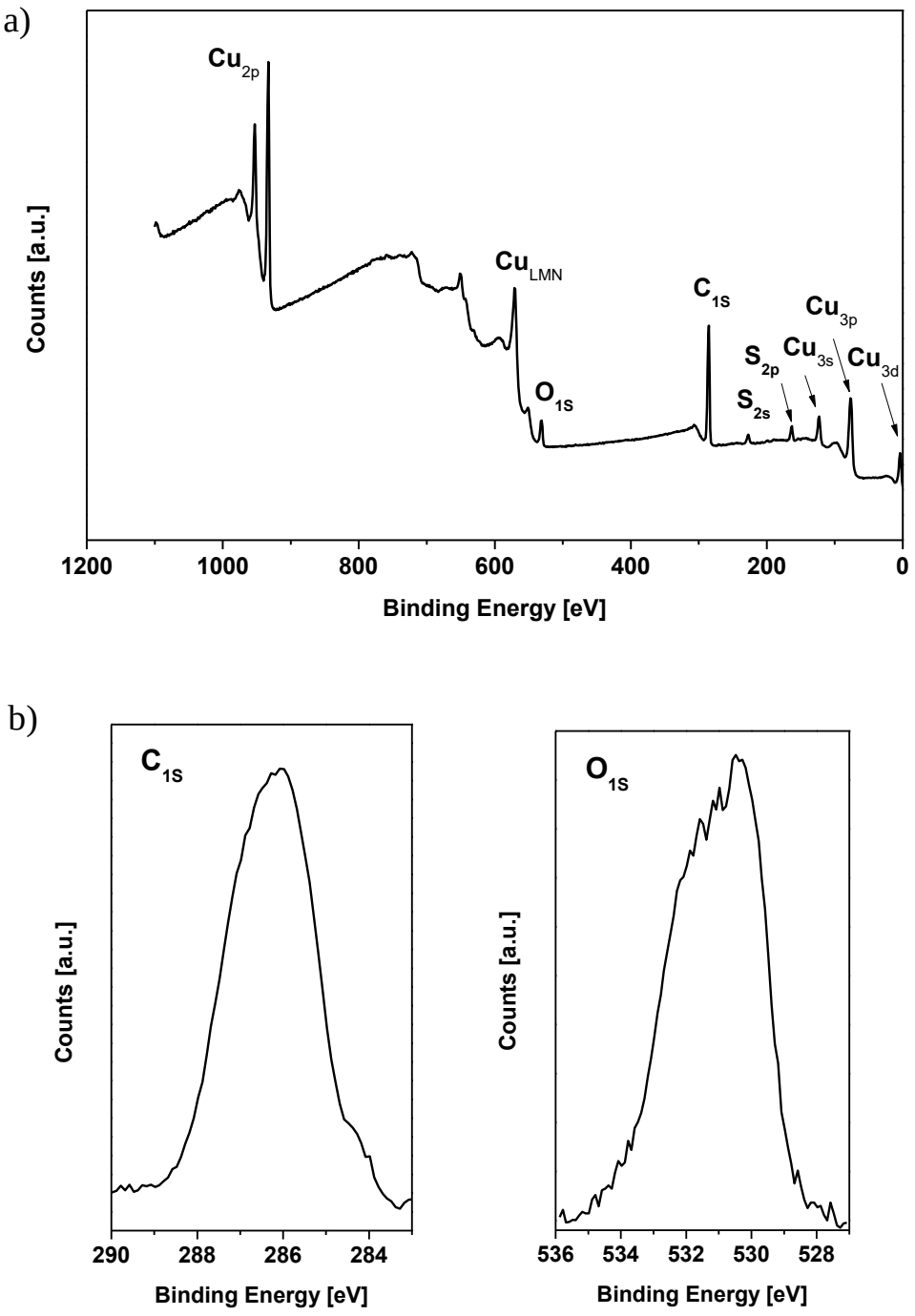

Figure S5. (a) XPS survey spectra (b) High resolution XPS spectra of C_{1s} and O_{1s}

7. Deconvolution of the Cu_{2p} XPS signal at 930 eV

Cu(I) and Cu(0) have almost the same XPS spectra; to distinguish the two oxidation degrees, the L3MM Auger band was acquired (see Fig SI.X1). Unfortunately, the spectrum shows a single broad peak (maximum at 917.4 eV), which makes it impossible to clearly discriminate between Cu(I) and Cu(0).
Therefore, and according to a reviewer's suggestion, we deconvoluted the Cu 2p XPS signal using two different contributions: the first one at 932.4 eV (Cu(0) or Cu(I)) and the second one at 934.1 eV (for Cu(II)) (see Fig. S7 and Table S1). From integration, At% of ca. 10% and 11% for respectively Cu(II) and Cu(0 or I) are obtained. The At% of oxygen (7.1%) is close to the value of Cu(II), which may indicate that CuO is the main oxidized form of Cu. This hypothesis is also supported by the fact that nanoparticles are subjected to well-known air-driven oxidation processes, responsible for the formation of Cu(II). In summary, Cu nanoparticles are likely composed of an equal amount of Cu(II) and Cu(0).

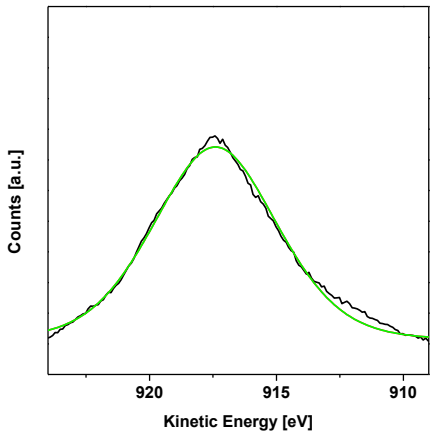

Fig. S6 : High resolution XPS spectra of Cu L3MM Auger band

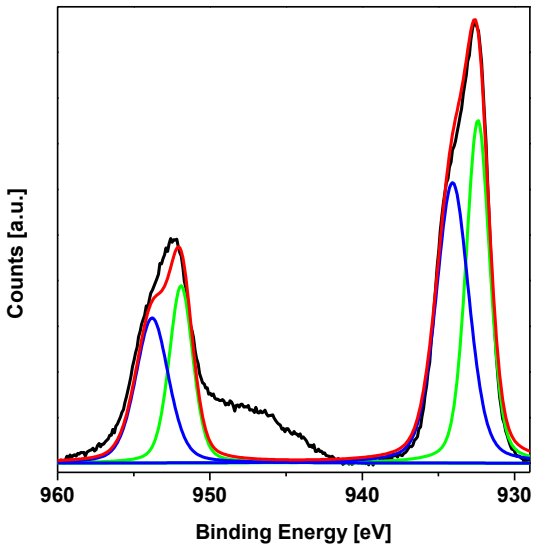

Fig. S7 : (black curve) High resolution XPS spectra of Cu2p, (red curve) simulated spectra from the fitting with (green and blue curves) two doublets.

Element		Peak BE (eV)	FWHM (eV)	Area (CPS.eV)	Atomic %
Cu(I or 0)	$2p_{1/2}$	932.4	1.83	163295	10.1
	$2p_{3/2}$	951.9	1.83	85616	
Cu(II)	$2p_{1/2}$	934.1	2.53	184036	9.9
	$2p_{3/2}$	953.8	2.53	96221	

Table S1: Cu_2p high resolution XPS spectra analysis

8. CuNPs prepared in the presence of 5 equiv. of PPh_3 at 65 °C without DDT.

(a) Cu/Phosphine = 1:5, 65 °C, 5 min

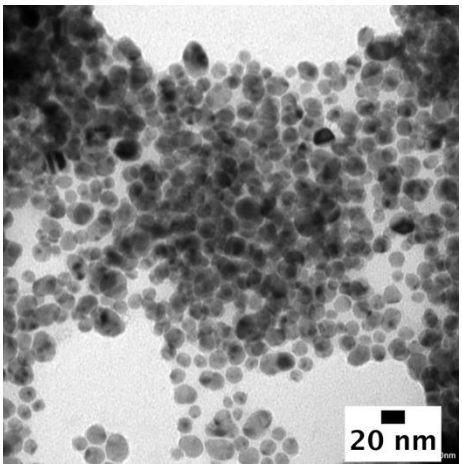

Mean size: 11 ± 2 nm (17 %)

(b) Cu/Phosphine = 1:5, 65 °C, 10 min

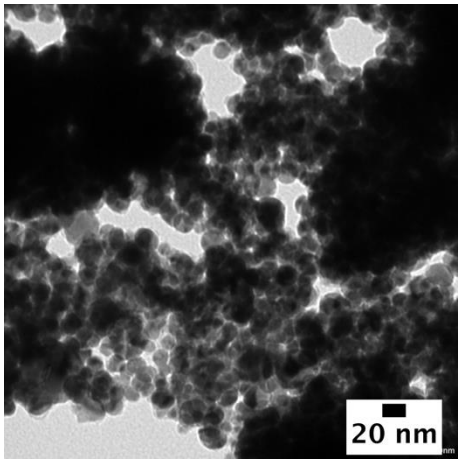

Mean size: 13 ± 2 nm (14 %)

(c) Cu/Phosphine = 1:5, 65 °C, 15 min

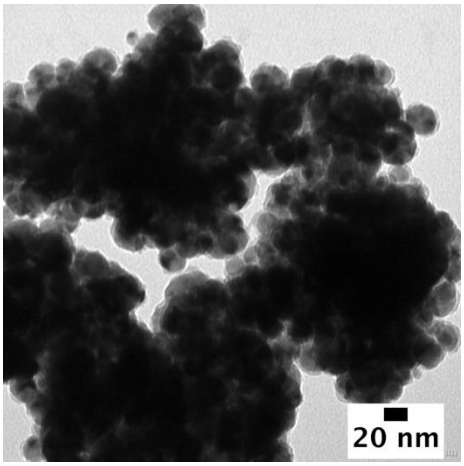

Mean size: 19 ± 4 nm (22 %)

(d) Cu/Phosphine = 1:5, 65 °C, 30 min

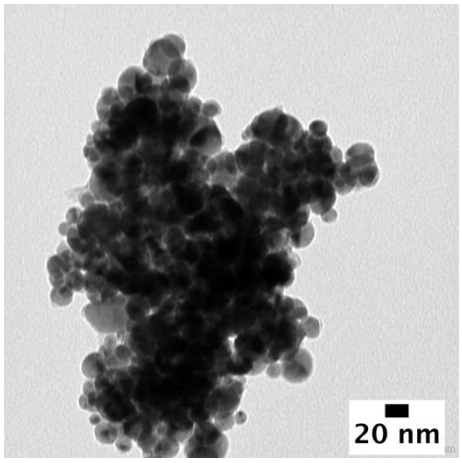

Mean size: 19 ± 4 nm (22 %)

Figure S8: TEM images of the NPs prepared with a copper-to-PPh_3 ratio of 1:5 at 65°C with different heating times without addition of DDT (a) 5 min (b) 10 min (c) 15 min (d) 30 min.

5 min	10 min	15 min	30 min
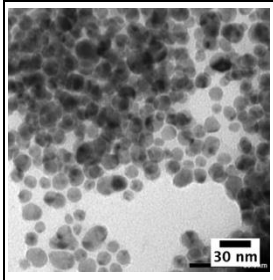	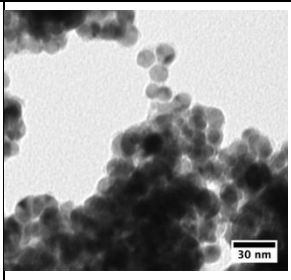	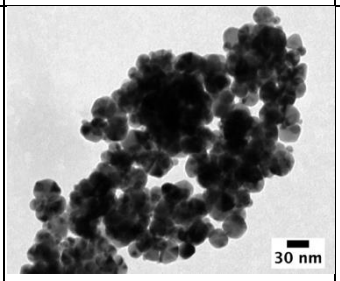	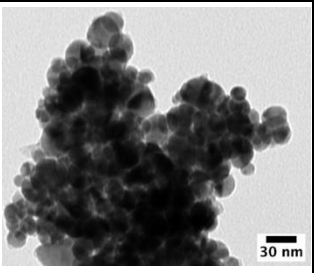
150-200 NPs measured by hand			

Figure S9: Examples of TEM images used to measure the size of the spheroids intermediates.

Figure S10. Photograph of CuNPs prepared in the presence of 5 equiv. of PPh_3 at 65 °C in $CHCl_3$ after centrifuging.

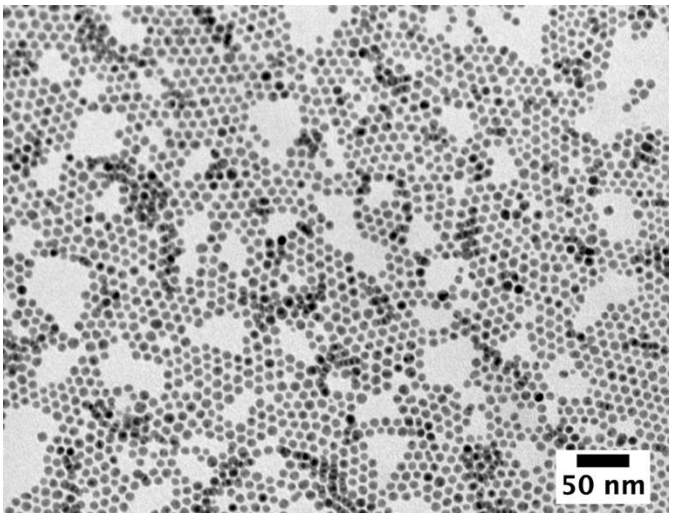

Figure S11. TEM image of CuNPs were characterized by XRD analysis which were prepared from the reaction condition of CuCl/*n*-BuMgCl/4 equiv. DDT at 65°C (in 5 mmol scale synthesis).